Polyoxometalates/TiO$_2$ Fenton-like photocatalysts with rearranged oxygen vacancies for enhanced synergetic degradation

Xiaoqiang An[a], Qingwen Tang[a,c], Huachun Lan[a,*], Huijuan Liu[a], Jiuhui Qu[a,b]

[a] Center for Water and Ecology, State Key Joint Laboratory of Environment Simulation and Pollution Control, School of Environment, Tsinghua University, Beijing 100084, China
[b] Key Laboratory of Drinking Water Science and Technology, Research Center for Eco-Environmental Sciences, Chinese Academy of Sciences, Beijing 100085, China
[c] College of Environmental Science and Engineering, Guilin University of Technology, Guilin 541006, China

ARTICLE INFO

ABSTRACT

Oxygen vacancy modulation has emerged as a prevalent strategy to improve the performance of heterogeneous catalysts. By far, the impact of oxygen vacancy rearrangement on the efficiency of Fenton-like reaction remains largely unknown. In this paper, Fe-containing polyoxometalates were coupled with defect-rearranged TiO$_2$ to construct defective Fenton-like photocatalysts. Experimental characterizations revealed that defect rearrangement facilitated the interfacial transfer of electrons from TiO$_2$ to polyoxometalate molecules. Fenton-like photocatalysts with rearranged defects exhibited 5 and 3.5 times higher activity for the synergetic degradation of toxic dye and 5-Sulfosalicylic acid than pristine TiO$_2$. This enhancement was ascribed to the beneficial role of oxygen vacancy modulation for activating oxygen and H$_2$O$_2$ molecules into $\cdot$O$_2^-$ and $\cdot$OH radicals. Our work provides new opportunities for exploring efficient Fenton-like photocatalysts for environmental remediation.

1. Introduction

As one of the most important advanced oxidation processes (AOPs), Fenton reaction is widely used in wastewater treatment. By far, the practical application of this classical technique is still limited by the narrow pH range, the generation of massive iron precipitations, and the slow transformation rate of Fe(III)/Fe(II) redox couples [1–4]. Therefore, the development of solid catalysts with wide working pH range for heterogeneous Fenton-like processes has become a hot research topic.

Although lots of iron-contained solid compounds have been explored as Fenton-like catalysts, the catalytic efficiency of these materials is still moderate [5,6]. The combination of Fenton-like reaction with other AOPs techniques is worthy of further exploration. Recently, light-assisted heterogeneous Fenton-like process has been considered as an effective method to improve the efficiency of degradation reaction. Many efforts have been made to construct Fenton-like photocatalysts, such as C$_3$N$_4$/FeOOH, TiO$_2$/Fe$_2$O$_3$, WO$_3$/Fe$_3$O$_4$ etc [7–11]. When a catalyst is used for H$_2$O$_2$ activation, the catalytic performance is usually highly dependent on the transfer efficiency of interfacial charge carriers. For example, Yin et al. reported that vacancy defects in metal sulfides could provide active sites for accelerating Fe^{3+}/Fe^{2+} conversion, which was the rate-limiting step of Fenton reaction [12]. Di J et al. reported that the presence of bismuth vacancies created a new defect

level in forbidden band and increased density of states at the valence band maximum, resulting in increased charge carrier concentration and electronic conductivity [13]. Our recent work also demonstrated that oxygen doping could result in the formation of strongly coupled heterostructured interfaces, which greatly facilitated the charge transfer from g-C$_3$N$_4$ to polyoxometalates [14]. Therefore, the strategically modulation of interfacial electronic structure of Fenton-like photocatalysts might release more unexploited room for the development of high-performance heterogeneous catalysts.

As one of the most important defects in metal oxides, oxygen vacancies have triggered an explosion of research interest with respect to the unpredictable properties. The critical role of oxygen vacancies during the separation of photocarriers has already been validated by both theoretical calculations and experimental observations [15–19]. Moreover, we found that the rearrangement of oxygen vacancy defects in nonstoichiometric oxides contributed to the superior photoactivity of defective TiO$_2$. The diminishment of bulk defects and preservation of surface oxygen vacancies led to the 12-fold increased activity for photocatalytic water reduction [20]. For Fenton-like reactions, although the oxygen vacancy-dependent generation of hydroxyl radicals has been revealed recently, the impact of defect rearrangement on the efficiency of hydrogen peroxide activation is still an open question [21–24]. In order to explore more efficient catalysts for AOPs, it is a

critical point to deliberate the combination of oxygen vacancy modulation with Fenton-like reactions.

With this in mind, we hypothesized the oxygen vacancy-mediated construction of defective TiO_2-based catalysts for Fenton-like photocatalysis. In this strategy, hydrogen and cyanide were sequentially used to provide the required atmosphere for oxygen vacancy generation and rearrangement, respectively. Based on the experimental characterizations, the rearranged oxygen vacancies contributed to the formation of defective electronic structure of Fenton-like catalysts. Benefited from the fast electron transfer from TiO_2 photocatalysts to polyoxometalates (POM) nanoparticles. When used as Fenton-like photocatalysts, composite catalysts with modulated oxygen vacancies exhibited 5 and 3.5 times higher activity for the synergetic degradation of toxic dye and 5-Sulfosalicylic acid (SSA) than pristine TiO_2. The enhancement was ascribed to the superior ability for generating $\cdot O_2^-$ and $\cdot OH$ reactive radicals. The underlying mechanism of defect-facilitated photo-Fenton-like reactions was fundamentally investigated.

2. Experimental section

2.1. Defect modulation of TiO₂ photocatalysts

A traditional hydrothermal method was firstly used to fabricate hydrogen titanate precursor. Typically, 1.5 g of commercial p25 TiO_2 was put into 30 ml of 10 M NaOH solution. The suspension was sonicated for 30 min and stirred for another 60 min to achieve good dispersity. Then, the solution was transferred into a 50 ml Teflon-lined autoclave. The hydrothermal reaction was carried out at 150℃ for 24 h. After filtration and washing, the dried precipitate was treated by 0.1 M hydrochloric acid and washed with DI water until the neutral pH value. The product was dried at 80 ℃ in a vacuum oven and calcined in a muffle furnace at 450 ℃ for 4 h to obtain TiO_2 nanofibers (denoted as TiO_2).

As-synthesized TiO_2 powders were further calcined at 450 ℃ for 4 h under H_2/Ar mixed gas condition in a tubular furnace, with a gas flow rate of 50 mL/min. This procedure resulted in the formation of non-stoichiometric TiO_2 with abundant oxygen vacancies (V_O-TiO_2). To achieve the rearrangement of oxygen vacancies, V_O-TiO_2 and a certain amount of cyanide were put into 30 ml of water under stirring. Then, the solution was dried overnight on a hot plate under strong stirring. Finally, the powders were placed into a muffle furnace and calcined at 550 ℃ for 4 h. This cyanide-assisted heat-treatment procedure facilitated the formation of TiO_2 with rearranged oxygen vacancies (R-V_O-TiO_2).

2.2. Fabrication of polyoxometalates/TiO₂ catalysts

An impregnation method was used to fabricate polyoxometalates/TiO_2 Fenton-like catalysts. In a typical procedure, 6 mg of $FeCl_3$ and 28 mg of $H_3PW_{12}O_{40}\cdot xH_2O$ were dissolved in 100 ml water, and the pH value was adjusted to 1 [28]. Then, 0.1 g of R-V_O-TiO_2 was added into as-formed solution. After 12 h of vigorous agitation, the precipitate was separated, washed and dried to obtain polyoxometalates/ TiO_2 nanocomposites (Fe-POM/ R-V_O-TiO_2).

2.3. Characterization

X-ray diffraction (XRD) patterns of the samples were recorded on a Rigaku RINT 2100, at a voltage of 40 kV. The morphology of the samples was observed by field emission scanning electron microscopy (FE-SEM, JSM-7600 F, JEOL) and high-resolution transmission electron microscopy (HR-TEM, JEOL-2100 F). X-ray photoelectron spectroscopy (XPS) was carried out using the XPS spectrometers (ESCALab220I-XL). UV–vis diffuse reflectance spectra (DRS) were collected by a UV–vis-NIR spectrometer (Cary 5000). Electron spin resonance (ESR) analysis was carried out by a Bruker E500 spectrometer. The steady-state

fluorescence and time-resolved fluorescence spectra were measured on a fluorescence spectrometer (FLS-980, Edinburgh Instruments Ltd.).

2.4. Photo-assisted Fenton-like degradation of pollutants

The pollutant removal ability of as-synthesized catalysts was evaluated by using toxic dye, sulfosalicylic acid (SSA) and bisphenol A molecules as typical contaminants in water. For the photo-assisted Fenton-like reactions, 50 mg catalysts and 50 mmol H_2O_2 were added into the solution of dye with the concentration of 20 mg/l or sulfosalicylic acid with the concentration of 10 mg/L. The suspension was ultrasonicated for 0.5 h and magnetically stirred for 1.5 h in the dark to achieve the adsorption/desorption equilibrium. Then, the solution was irradiated by a xenon lamp (CEL-S500, 300 W). The light density was determined to be 200 mw/cm². At given time intervals, 3 ml liquids were collected and filtered by 0.45 μm filtration membrane for analysis. The concentration of dyes was analyzed by measuring the absorption of pollutant solution, using a UV/Vis spectrophotometer (Hitachi, Japan). The SSA concentration was analyzed by a high-performance liquid chromatogram (HPLC) (Agilent, USA). The removal ratio of pollutant molecules was calculated by C/C_0, where C was the concentration of pollutant at each irradiated time interval and C_0 was the initial concentration of pollutant solution. To verify the active oxygen radicals, the ESR signals of radicals spin-trapped by 5,5-dimethyl-1-pyrrolin-*N*-oxide (DMPO) were recorded during photodegradation reactions. For the evaluation of catalytic stability, the catalyst was collected by centrifugation and washed with DI water several times after the degradation of methylene blue molecules. The dried powders were directly used as Fenton-like photocatalysts for the next run.

2.5. Photoelectrochemical measurements

The electrodes were prepared by a drop-casting method. Potentiostatic electrical impedance spectroscopic (EIS) and Mott-Schottky measurements were carried out using a three-electrode setup. Pt wire and Ag/AgCl electrode were used as the counter and reference electrodes, respectively. 0.5 M Na_2SO_4 solution was used as electrolyte. EIS spectra were recorded under an AC perturbation signal of 5 mV over the frequency range from 1 MHz to 100 mHz.

3. Results and discussion

Measurements were carried out to clarify the structure of iron-containing polyoxometalates (Fig. S1). Series of peaks were observed in the XRD pattern of blank Fe-POM (Fig. S2), suggesting the formation of Keggin-ype phosphotungstate [25]. According to the survey XPS result (Fig. S3a), Fe, W, P and O were determined to be the dominant component elements of Fe-POM nanoparticles. High-resolution Fe 2p and W 4f spectra revealed that the valence states of iron and tungsten were III and VI, respectively. Combined with the W-O-O-W, W=O and W−P−O bonds in the O 1 s spectrum, the successful formation of Keggin-type Fe (III){PO_4[$WO(O_2)_2$]$_4$} could be deduced, which is consistent with the previous research [26]. The phase structure of composite catalysts were thereafter investigated. As can be seen from Fig. 1, all samples presented similar diffraction peaks at 25.4, 37.8, 48.2, 53.8, 55.08 62.7, 68.8 and 70.4°, corresponding to anatase phase of TiO_2 (JCPDS 21-1272). It indicates that the formation and rearrangement of oxygen vacancies showed negligible influence on the crystal phase of catalysts. Moreover, the typical peaks of Fe-contained POM were not observed, due to the high dispersity and relatively low amount in the composites.

Fig. S5a shows the SEM images of as-prepared TiO_2 photocatalysts fabricated from hydrogen titanate precursor. A large number of 1-D nanofibers were clearly observed, which were self-assembled into a 3-D porous network to reduce the surface energy. After the thermal reduction, the 1-D fibrous morphology of TiO_2 was mainly preserved (Fig. S5b). In contrast, the cyanide-assisted heat-treatment led to the collapse
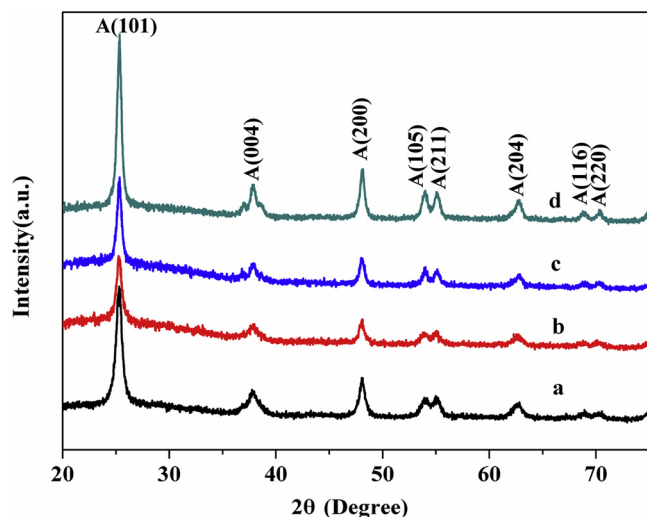
Fig. 1. XRD patterns of different catalysts. a: TiO_2, b: V_O-TiO_2, c: R-V_O-TiO_2, d: Fe-POM/ R-V_O-TiO_2.

of 1-D fibrous structure, whereafter forming POM/TiO_2 nanoparticles (Fig. S5c and S5d). The morphology of catalysts was further investigated by TEM characterizations. For 1-D TiO_2 in Fig. 2a, the average diameter and length of nanofibers were about 9 nm and several hundreds of nanometers, respectively. In the HR-TEM image (Fig. 2b), the lattice fringe with the interplanar spacing of 0.35 nm and 0.235 nm could be indexed to the (101) and (001) planes of anatase TiO_2, which was consistent with the XRD results [27]. No obvious change of dominant lattice spaces was observed during the defect modulation procedures. However, the occurance of amorphous layer on the surface of hydrogen-treated sample indicated the formation of oxygen-deficient structure (Fig. 2c). Due to the corrosive atmosphere caused by cyanamide decomposition, collapse of 1-D fibrous framework led to the formation of abundant TiO_2 nanoparticles with an average diameter of 15 nm. The clear lattice space and the decreased thickness of amorphous layer indicated the restoration of electronic structure, which was consistent with our previous results [20]. The representative TEM image of Fe-POM/R-V_O-TiO_2 composites is presented in Fig. 2g. Besides the typical structure of R-V_O-TiO_2, a large number of nanoclusters, with average diameter of less than 1 nm, were observed. According to Fig. S6, increasing the concentration of Fe-POM precursor resulted in the increase of nanocluster amount. EDS mapping analysis revealed that the distribution of Fe, W and O signals in the composites was uniform (Fig. S7). All these results indicated the successful immobilization of highly

dispersed Fe-POM onto the surface of TiO_2 (Fig. 2h) [28,29].

The electronic structure of as-synthesized catalysts during the defect modulation procedures was studied by ESR, a sensitive technique for detecting oxygen vacancy-induced electrons and surface defects. In Fig. 3a, no obvious ESR signal was detected for pristine TiO_2. As expected, a strong paramagnetic peak centered at g value of 1.997 was observed for Vo-TiO_2. It indicated that abundant oxygen vacancy defects formed during the thermal reduction treatment [30]. The obviously decreased ESR signal of cyanamide treated sample (R-V_O-TiO_2) well confirmed the partial restoration of defective structure, i.e. the rearrangement of oxygen vacancies. This defect rearrangement process exhibited obvious impact on the interfacial charge transfer in Fe-POM/R-V_O-TiO_2 composites. The decreased ESR signal intensity indicated that defect-induced electrons migrated from TiO_2 to Fe-POM, i.e. polyoxometalate acted as electron shuttle to enhance the charge separation [31–33].

The influence of oxygen vacancies on the optical absorption of catalysts was investigated by UV–vis DRS. In Fig. 3b, TiO_2 with intrinsic wide bandgap only responded to ultraviolet light. The formation of new defect energy levels in Vo-TiO_2 resulted in a large absorption tail in the visible light region, with a decreased bandgap of 2.75 eV (Fig. S8). Due to the restoration of oxygen vacancies, the visible light absorption of R-Vo-TiO_2 obviously decreased. Moreover, a slightly widened bandgap (3.06 eV) was observed for R-Vo-TiO_2 with rearranged defects. The changed color of powders from white to gray and light yellow well supported the above results (inset of Fig. 3b). The immobilization of small amount of Fe-POM showed ignorable influence on the optical property of catalysts.

The impact of defect modulation on the bonding environment of component elements was studied by XPS. In the Ti 2p spectrum of pristine TiO_2, the peaks centered at 458.5 eV and 464.1 eV could be ascribed to Ti $2p_{3/2}$ and Ti $2p_{1/2}$, respectively (Fig. 4a). Although ESR technique provided concrete evidence for the formation and rearrangement of oxygen vacancies, no peaks corresponding to Ti^{3+} was observed in the Ti spectrum of TiO_2 photocatalysts. This was consistent with previous reports that surface Ti^{3+} was prone to be neutralized by oxygen molecules in the atmosphere [34]. As a result, changes in the quantity of oxygen vacancies were not reflected by surface-sensitive XPS technique. However, when defective TiO_2 was coupled with Fe-POM nanoparticles, an obvious peak shift towards higher binding energy was achieved. This phenomenon indicated that free electrons caused by oxygen vacancies were effectively trapped by polyoxometalates molecules. Accordingly, the strong interfacial interactions between TiO_2 and Fe-POM presented great impact on the electronic structure of Fe-POM. In the high resolution W 4f spectrum of Fe-POM/R-V_O-TiO_2, two asymmetrical peaks could be easily observed. The two
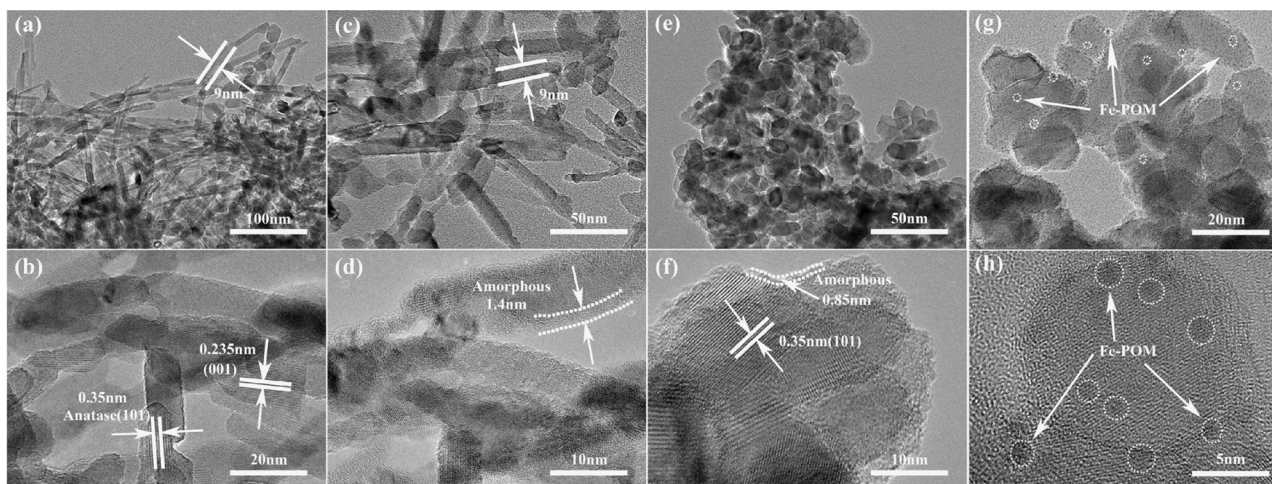

Fig. 2. TEM and HR-TEM images of TiO_2 (a, b); V_O-TiO_2 (c, d); R-V_O-TiO_2 (e, f); Fe-POM/R-V_O-TiO_2 (g, h).
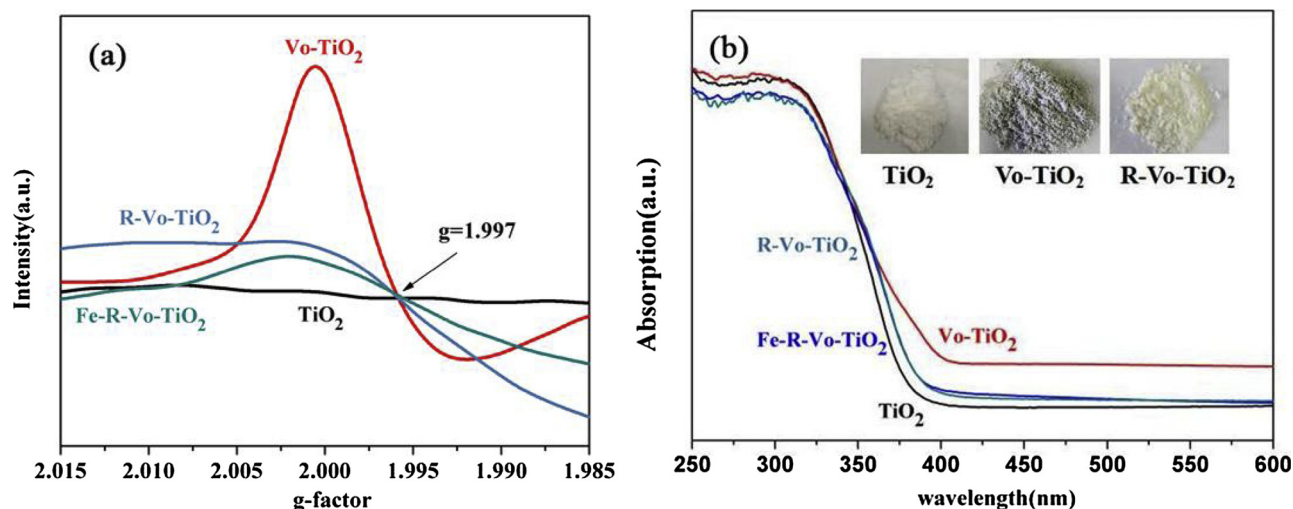
Fig. 3. (a) ESR spectra of TiO_2, V_O-TiO_2, R-V_O-TiO_2 and Fe-POM/ R-V_O-TiO_2; (b) DRS spectra of TiO_2, V_O-TiO_2, R-V_O-TiO_2 and Fe-POM/ R-V_O-TiO_2.

strong peaks located at 35.7 and 37.8 eV were ascribed to W $4f_{7/2}$ and W $4f_{5/2}$ of W^{6+}. The appearance of additional peaks at 37.2 indicated the formation of W^{5+}.[15] This was quite different from the symmetrical W 4f peaks of pristine POM nanoparticles (Fig. S4b). It indicated that the strategically modulation of oxygen vacancies and the construction of heterostructured interface could greatly facilitate the charge transfer from TiO_2 to POM molecules. Note that the favorable role of reduced W^{5+} as active catalytic sites has been revealed by our recent research, superior catalytic activity was reasonably anticipated for Fe-POM/R-Vo-TiO_2 [14].

The applicability of defect-modulated catalysts for photo-assisted heterogeneous Fenton-like reaction were evaluated by degrading organic pollutants under simulated solar light. Methylene blue (MB) was firstly selected as target pollutant for degradation reaction. As shown in Fig. 5a, the photoactivity of pristine TiO_2 was poor, as only 48% MB was degraded after 12 min. Although the addition of H_2O_2 into the photocatalytic system contributed to the improved activity of R-Vo-TiO_2, its dye removal ability was still moderate. In contrast, the co-existence of Fe-POM and H_2O_2 resulted in the significantly improved catalytic performance, indicating the synergetic effect between photocatalysis and heterogenous Fenton-like reactions. Compared to pristine TiO_2, the 5-fold enhanced MB removal rate demonstrated the great potential of Fenton-like photocatalysts.

The influence of experimental conditions on the performance of composite catalysts was further investigated. As shown in Fig. 5b, no

noticeable degradation of MB was observed for Fe-POM/R-Vo-TiO_2 catalysts without light irradiation, verified the hypothesis of light-assisted Fenton-like reaction. Moreover, the average apparent rate constant of Fe-POM/R-Vo-TiO_2 was 3.2 times higher than that of Fe-POM/ TiO_2. It indicated that oxygen vacancy modulation of TiO_2 photocatalysts indeed contributed to the superior activity of Fenton-like catalysts. Thanks to the unique interfacial charge transfer, Fe-POM/R-Vo-TiO_2 with modulated defects also exhibited 5.6 times higher activity than Fe-POM/P25 catalysts. Control experiments indicated that the activity of defective Fenton-like photocatalysts was influenced by the precursor used for oxygen vacancy rearrangement. In Fig. S9, Fe-POM/ R-Vo-TiO_2 fabricated from cyanide presented the highest activity for MB degradation.

To exclude the possible photosensitization effect of heterocyclic dye molecules under visible light irradiation, the activity of as-synthesized Fenton-like photocatalysts was further evaluated by degradating colorless pollutants. 5-Sulfosalicylic acid (SSA) and bisphenol A (BPA), typical chemicals that might cause serious damage to human beings, were used as model pollutants. In Fig. S10, R-V_O-TiO_2 exhibited 3-fold improved activity than pristine TiO_2 for photodegradating BPA. This further confirmed the significant contribution of oxygen vacancy rearrangement process to the photocatalytic reaction. Similar trend was also observed during the photodegradation of SSA. The activity of Fe-POM/R-V_O-TiO_2 was 2.7 and 3.5 times higher than R-V_O-TiO_2 and pristine TiO_2, respectively (Fig. 5c). These results confirmed the
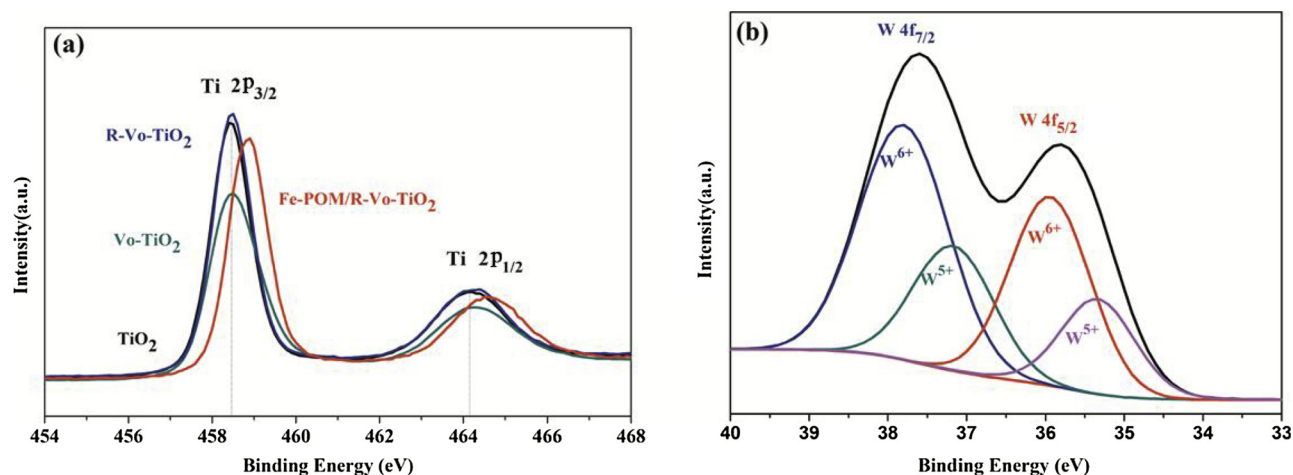

Fig. 4. (a) Ti 2p spectra of TiO_2, V_O-TiO_2, R-V_O-TiO_2 and Fe-POM/R-V_O-TiO_2. (b) High resolution W 4f spectra of Fe-POM/R-V_O-TiO_2.
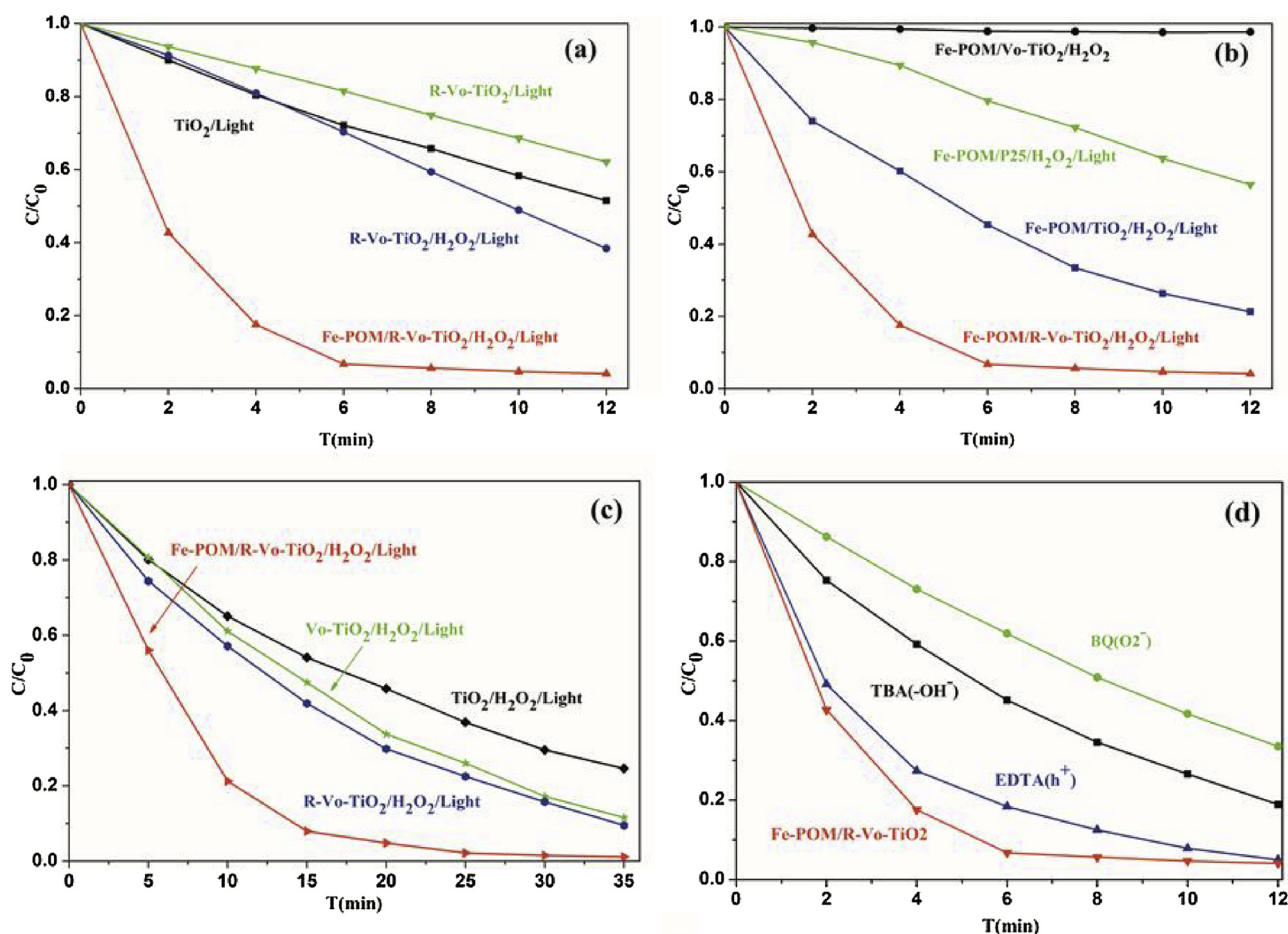
Fig. 5. (a) Comparison of different catalytic reactions for degradating MB dyes; (b) Influence of defective structure of TiO_2 on the degradation of MB dyes; (c) Influence of defective structure of TiO_2 on the degradation of SSA; (d) Degradation of MB dyes over Fe-POM/R-Vo-TiO_2 in the presence of different scavengers.

superior performance of our Fenton-like photocatalysts with modulated defects.

In addition, the stability of the composite catalysts was evaluated by degrading MB for cycle runs. As shown in Fig. S11, the hybrid catalyst was reusable and the removal efficiency was maintained in the fourth recycling test. The slight drop of degradation efficiency was ascribed the weight loss of catalyst in the progress of collection and the possible residual of dye molecules or intermediate products after heterogenous catalysis (as evidenced by Fig. S12). Therefore, as-prepared Fe-POM/R-V_o-TiO_2 has high photocatalytic stability and recyclability.

To gain fundamental insights into the mechanism of Fenton-like photocatalytic reactions, active species trapping experiments were firstly carried out. Ethylene diamine tetraacetic acid disodium salt (EDTA-2Na), benzo quinone (BQ) and tert-butyl alcohol (TBA), typical scavengers for hole, superoxide and hydroxyl radicals, were added into the reaction solution to remove the corresponding reactive species. When EDTA-2Na was added, the degradation of MB was almost invariable (Fig. 5d). Therefore, photo-induced holes were not the major reactive species for pollutant removal. However, the addition of BQ resulted in a sharp decrease of degradation efficiency. Decreased removal ratio was also observed after the addition of TBA. These results suggests that $\cdot O_2^-$ and $\cdot OH$ were the dominant reactive species for the oxidation reaction over Fe-POM/R-V_o-TiO_2 catalysts [35]. In general, the generation of reactive species is strongly dependent with the electronic structure of catalysts. With regard to our Fenton-like photocatalysts, the generation and rearrangement of oxygen vacancies was favorable for the fast transportation of photo-generated electrons [17]. Thus, an obvious decrease of plot slop, i.e. increased electron density, was obtained in the Mott-Schottky plot of R-V_o-TiO_2 (Fig. S13). Due to

the efficient separation of electrons, TiO_2 with modulated defects presented superior activity for photoreduction reactions. This was reflected in the significantly improved hydrogen evolution activity, which agreed well with our previous reports (Fig. S14) [20]. Thus, it is not difficult to understand the enhanced ability of R-V_o-TiO_2 for activating oxygen molecules into $\cdot O_2^-$. The significantly increased ESR signal of $\cdot O_2^-$ further evidenced the above deduction (Fig. 6a) [36].

Grafting Fe-POM nanoclusters onto oxygen-deficient TiO_2 resulted in the formation of strongly coupled heterojunction. PL and time-resolved photoluminescence (TRPL) decay spectra were used to investigate the charge transfer behavior around heterostructured interface. Based on the PL spectra in Fig. S15a, TiO_2 exhibited a strong emission peak, which is characteristic of the radiative recombination of charge carriers. Remarkably, the emission intensity decreased after the rearrangement of oxygen vacancies. The loading of Fe-POM further quenched the emission peak, i.e. photo-induced electrons could further transfer from R-V_o-TiO_2 to POM molecules. It indicated that the charge carriers in Fe-POM/R-V_o-TiO_2 were efficiently separated, leading to much stronger surface photovoltage response in the surface photovoltage measurement (Fig. 6b). [37], Accordingly, the facilitated charge transfer decreased interfacial conductivity, and much smaller arc radius of Fe-POM/R-V_o-TiO_2 was achieved in the EIS results (6c) [38].

To gain more insight into the charge transfer dynamics, TRPL decay measurements were carried out. As shown in Fig. S15b, all curves could be fitted well to a triexponential decay function, with all the fitting parameters summarized in Table S1. As reported previously, the fast component ($\tau 1$) corresponds to the direct formation of free electrons/holes, whereas the slow component ($\tau 2$, $\tau 3$) originates from indirect
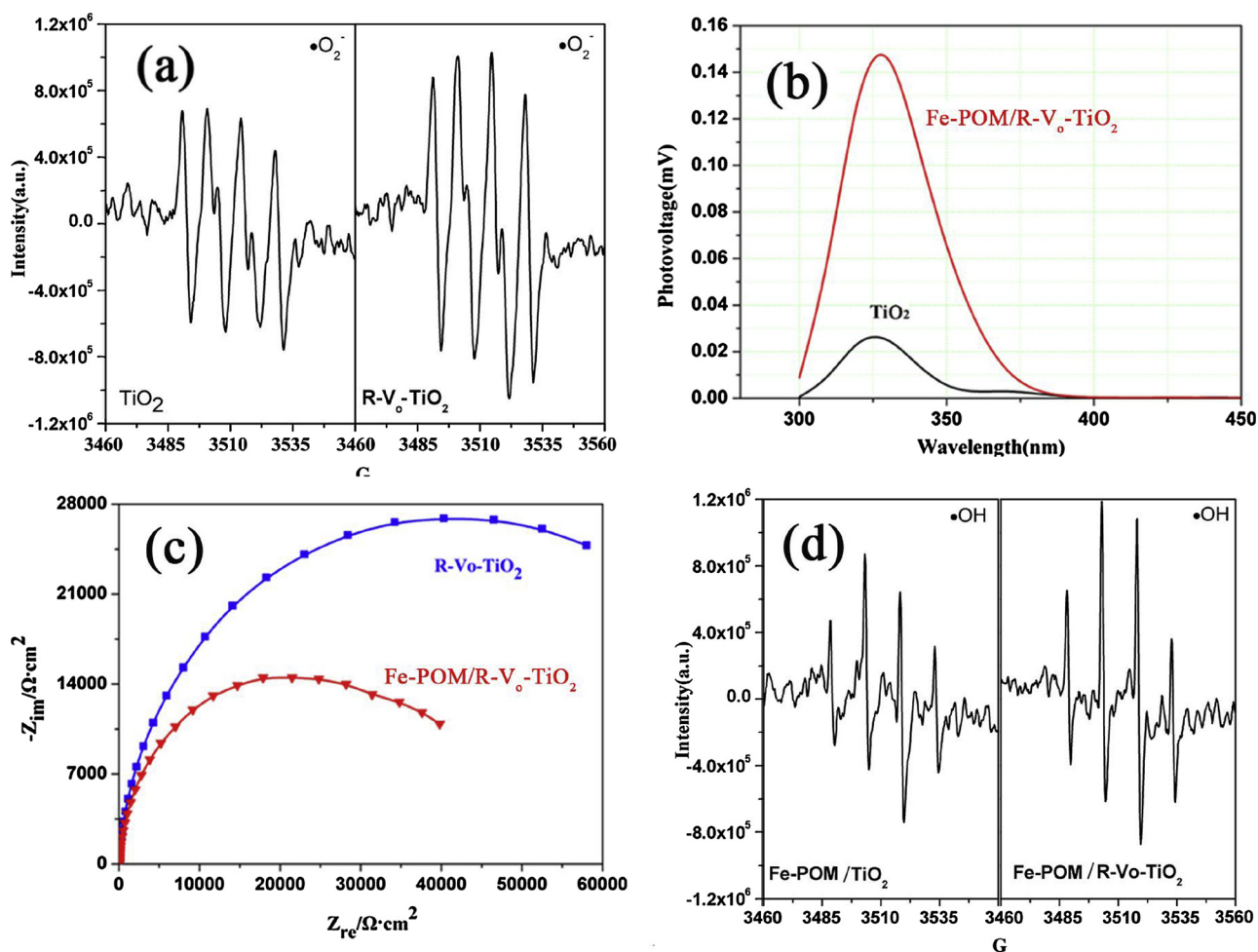
Fig. 6. (a) ESR spectra of DMPO-$\cdot$O$_2^-$ adducts in aqueous solution over TiO$_2$ and R-V$_o$-TiO$_2$; (b) Surface photovoltage spectra of TiO$_2$ and Fe-POM/R-Vo-TiO$_2$; (c) EIS spectra of R-Vo-TiO$_2$ and Fe-POM/R-Vo-TiO$_2$; (d) ESR spectra of DMPO-$\cdot$OH adducts in aqueous solution over Fe-POM/TiO$_2$ and Fe-POM/R-V$_o$-TiO$_2$.
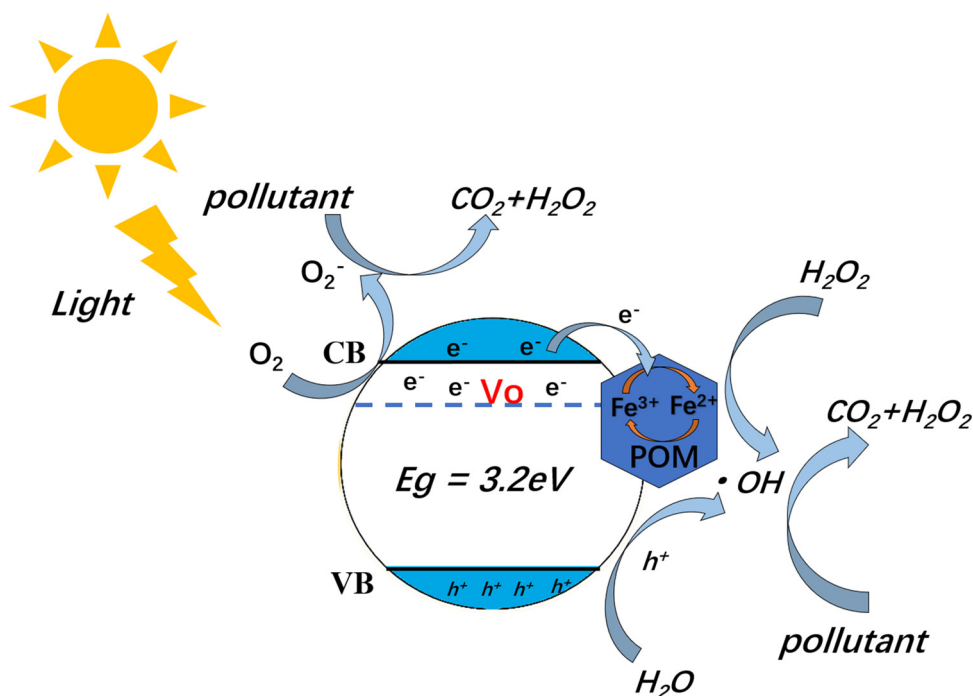

Fig. 7. Schematic illustration of photo-assisted Fenton-like reaction for contaminant removal.

formation of self-trapped excitons with trapped electrons [39]. The rearrangement of oxygen vacancies and subsequent loading of Fe-POM molecules resulted in the gradual both decrease of $\tau 1$ and $\tau 2$, suggesting the improved charge separation efficiency. Moreover, the electron transfer from defect-rearranged TiO_2 facilitated the formation of defective Fenton-like catalysts. The reduced metal ions in POM with low-valence states could act as new reactive sites for the generation of ·OH [13]. As a result, much stronger ESR signal of ·OH was detected over the surface of Fe-POM/R-Vo-TiO_2 (Fig. 6d).

Based on these results, a hypothetic schematic illustration of photo-assisted Fenton-like mechanism is presented in Fig. 7. Firstly, photo-induced electrons were effectively separated through oxygen vacancy modulation and heterostructure construction [40,41]. As a result, abundant ·O_2^- formed, which acted as the dominant reactive radicals for the photodegradation of organic pollutants. Secondly, ·OH were partially generated through the photooxidation of water by separated holes in TiO_2. Moreover, iron ions in POM could also act as reactive sites for generating ·OH through heterogeneous Fenton-like reactions. Thirdly, efficient transfer of photo-induced electrons from TiO_2 to Fe-POM accelerated the Fe^{3+}/Fe^{2+} conversion [42]. Thus, the synergetic effect between photocatalysis and Fenton-like reaction significantly contributed to the superior activity of catalysts for pollutant removal.

4. Conclusions

In summary, we demonstrated that defect modulation could provide an effective way to improve the synergetic effect between photocatalysis and Fenton-like reactions. Experimental characterizations evidenced that rearrangement of oxygen vacancies was favorable for the electron transfer from TiO_2 to Fe-POM, resulted in the formation of defective composite catalysts. The facilitated activation of oxygen molecules and the accelerated Fe^{3+}/Fe^{2+} conversion contributed to the significantly improved activity of as-developed catalysts for degrading toxic dye and SSA pollutants. The impressive improvement was attributed to the facilitated separation of charge carriers and the synergetic effect between photocatalysis and Fenton-like reactions. Thus, our study demonstrated a feasible way for developing more efficient Fenton-like catalysts through defect modulation.

Acknowledgments

Appendix A. Supplementary data

Supplementary material related to this article can be found, in the online version, at doi:https://doi.org/10.1016/j.apcatb.2018.11.063.

References

[1] L. Doumic, P. Soares, M. Ayude, M. Cassanello, R. Boaventura, V. Vilar, Chem. Eng. J. 277 (2015) 86–96.
[2] G. Ruppert, R. Bauer, G. Heisler, Chemosphere 28 (1994) 1447–1454.
[3] K. Wu, Y. Xie, J. Zhao, H. Hidaka, J. Mol. Catal. A Chem. 144 (1999) 77–84.
[4] M. Ortega-Liébana, E. Sánchez-López, J. Hidalgo-Carrillo, A. Marinas, J. Marinas, F. Urbano, Appl. Catal. B-Environ. 127 (2012) 316–322.
[5] M. Yoon, Y. Oh, S. Hong, J. Lee, R. Boppella, S. Kim, F. Mota, S. Kim, D. Kim, Appl. Catal. B-Environ. 206 (2017) 263–270.
[6] N. Wang, Y. Du, W. Ma, P. Xu, X. Han, Appl. Catal. B-Environ. 210 (2017) 23–33.
[7] K. Sahel, L. Elsellami, I. Mirali, F. Dappozze, M. Bouhent, C. Guillard, Appl. Catal. B-Environ. 188 (2016) 106–112.
[8] C. Ruales-Lonfat, J.F. Barona, A. Sienkiewicz, M. Bensimon, J. Vélez-Colmenares, N. Benítez, C. Pulgarín, Appl. Catal. B-Environ. 166–167 (2015) 497–508.
[9] K. Lee, X. Chuah, Y. Cheng, S. Lu, J. Mater. Chem. A 3 (2015) 18578–18585.
[10] W. Luo, L. Zhu, N. Wang, H. Tang, M. Cao, Y. She, Environ. Sci. Tech. 44 (2010) 1786–1791.
[11] M. Yoon, Y. Oh, S. Hong, J. Lee, R. Boppella, S. Kim, F. Mota, S. Kim, D. Kim, Appl. Catal. B-Environ. 206 (2017) 263–270.
[12] M. Xing, W. Xu, C. Dong, Y. Bai, J. Zeng, Y. Zhou, J. Zhang, Y. Yin, Chem 4 (2018) 1359–1372.
[13] J. Di, C. Chen, C. Zhu, M. Ji, J. Xia, C. Yan, W. Hao, S. Li, H. Li, Z. Liu, Appl. Catal. B-Environ. 238 (2018) 119–125.
[14] X. An, S. Wu, Q. Tang, H. Lan, Y. Tang, H. Liu, J. Qu, Catal. Commun. 112 (2018) 63–67.
[15] X. An, B. Wen, J. Tang, Z. Hu, L. Liu, J. Qu, C. Huang, H. Liu, Adv. Energy Mater. 6 (2016) 1502268.
[16] X. An, L. Zhang, B. Wen, Z. Gu, L. Liu, J. Qu, H. Liu, Nano Energy 35 (2017) 290–298.
[17] T. Wei, Y. Zhu, Z. Gu, X. An, L. Liu, Y. Wu, H. Liu, J. Tang, J. Qu, Nano Energy (2018) 764–773.
[18] Y. Lu, Y. Huang, Y. Zhang, J. Cao, H. Li, C. Bian, S. Lee, Appl. Catal. B-Environ. 231 (2018) 357–367.
[19] C. Li, Z. Sun, A. Song, X. Dong, S. Zheng, D. Dionysiou, Appl. Catal. B-Environ. 236 (2018) 76–87.
[20] X. An, C. Hu, H. Liu, J. Qu, J. Mater. Chem. A 5 (2017) 24989–24994.
[21] H. Li, J. Shang, Z. Yang, W. Shen, Z. Ai, L. Zhang, Environ. Sci. Technol. 51 (2017) 5685–5694.
[22] G. Fang, Y. Deng, M. Huang, D. Dionysiou, C. Liu, D. Zhou, Environ. Sci. Technol. 52 (2018) 2178–2185.
[23] H. Jin, X. Tian, Y. Nie, Z. Zhou, C. Yang, Y. Li, L. Lu, Environ. Sci. Technol. 51 (2017) 12699–12706.
[24] Z. Lian, W. Wang, G. Li, F. Tian, K. Schanze, H. Li, ACS Appl. Mater. Interfaces 9 (2017) 16959–16966.
[25] X. Li, H. Xue, H. Pang, Nanoscale 9 (2017) 216–222.
[26] J. Liu, S. Xie, Z. Geng, K. Huang, L. Fan, W. Zhou, L. Qiu, D. Gao, L. Ji, L. Duan, L. Lu, W. Li, S. Bai, Z. Liu, W. Chen, S. Feng, Y. Zhang, Nano Lett. 16 (2016) 6568–6575.
[27] H. Zhang, J. Cai, Y. Wang, M. Wu, M. Meng, Y. Tian, X. Li, J. Zhang, L. Zheng, Jiang, J. Gong, Appl. Catal. B-Environ. 220 (2018) 126–136.
[28] J. Gunjakar, T. Kim, I. Kim, J. Lee, S. Hwang, Sci. Rep. 3 (2013) 2080.
[29] S. Liu, D. Kurth, B. Bredenkötter, D. Volkmer, J. Am. Chem. Soc. 124 (2002) 12279–12287.
[30] X. Chen, L. Liu, P. Yu, S. Mao, Science 331 (2011) 746–749.
[31] J. Ryu, W. Choi, Environ. Sci. Technol. 38 (2004) 2928–2933.
[32] C. Chen, P. Lei, H. Ji, W. Ma, J. Zhao, Environ. Sci. Technol. 38 (2004) 329–337.
[33] R. Ozer, J. Ferry, Environ. Sci. Technol. 35 (2001) 3242–3246.
[34] Y. Zhao, G. Chen, T. Bian, C. Zhou, G. Waterhouse, L. Wu, C. Tung, L. Smith, D. O'Hare, T. Zhang, Adv. Mater. 27 (2015) 7824–7831.
[35] Y. Wang, X. Zhao, D. Cao, Y. Wang, Y. Zhu, Appl. Catal. B-Environ. 211 (2017) 79–88.
[36] X. Kong, Y. Xu, Z. Cui, Z. Li, Y. Liang, Z. Gao, S. Zhu, X. Yang, Appl. Catal. B-Environ. 230 (2018) 11–17.
[37] T. Ma, J. Ran, S. Dai, M. Jaroniec, S. Qiao, Angew. Chem. Int. Ed. 54 (2015) 4646–4650.
[38] S. Gao, B. Gu, X. Jiao, Y. Sun, X. Zu, F. Yang, W. Zhu, C. Wang, Z. Feng, B. Ye, Y. Xie, J. Am. Chem. Soc. 139 (2017) 3438–3445.
[39] K. Zhang, L. Wang, J. Kim, M. Ma, G. Veerappan, C. Lee, K. Kong, H. Lee, J. Park, Energy Environ. Sci. 9 (2016) 499.
[40] S. Wang, S. Lin, D. Zhang, G. Li, M. Leung, Appl. Catal. B-Environ. 215 (2017) 85–92.
[41] D. Pan, Z. Han, Y. Miao, D. Zhang, G. Li, Appl. Catal. B-Environ. 229 (2018) 130–138.
[42] S. Giannakis, M. PoloLópez, D. Spuhler, J. Pérez, P. Ibáñez, C. Pulgarin, Appl. Catal. B-Environ. 199 (2016) 199–223.